

Essay

# Experimental Study on the Coefficient of Internal Frictional Resistance in the Annular Gap during the Plunger Gas Lift Process

Haowen Shi <sup>1,2</sup>, Zhong Chen <sup>1,3,\*</sup>, Ruiquan Liao <sup>1,2</sup>, Jie Liu <sup>1,2</sup>, Junliang Li <sup>1,2</sup> and Shan Jin <sup>4</sup>

<sup>1</sup> Hubei Key Laboratory of Oil and Gas Drilling and Production Engineering, Yangtze University, Wuhan 430100, China; 18592092302@163.com (H.S.); liaoruiquan@263.net (R.L.); liujie@yangtzeu.edu.cn (J.L.); lijunliang01@163.com (J.L.)

<sup>2</sup> Laboratory of Multiphase Pipe Flow, Gas Lift Test Base of CNPC, Wuhan 430100, China

<sup>3</sup> School of Information and Mathematics, Yangtze University, Jingzhou 434000, China

<sup>4</sup> Pipe China, Guiyang Oil and Gas Transmission Branch of Southwest Pipeline Company, Guiyang 550000, China; sechoned@163.com

\* Correspondence: 13571868528@163.com; Tel.: +86-135-7186-8528

**Abstract:** Plunger gas lift process technology is an economical solution to the problem of gas well liquid buildup. However, in-house simulation experiments revealed that the high-speed movement of the plunger may lead to fluid leakage and generate annular gap frictional resistance. To address this issue, a detailed experimental study was conducted to comparatively analyze five existing frictional-resistance models, which were found to have significant deviations. Therefore, we propose a new model of annular gap frictional resistance and validate it with experimental data, and the results show that the new model is more accurate and reliable. We also conducted a comparative analysis of production-site examples by using VB programming and found that when considering the annular gap frictional resistance, the upward travel time of the plunger was delayed, the difference between the upper and lower end face pressures was significant, and the difference in speed was 1.73 m/s. This indicates that the annular gap frictional resistance cannot be ignored and is crucial for optimizing plunger gas lift process technology and improving the drainage efficiency of gas wells.

**Keywords:** plunger gas lift; lifting experiments; coefficient of resistance



**Citation:** Shi, H.; Chen, Z.; Liao, R.; Liu, J.; Li, J.; Jin, S. Experimental Study on the Coefficient of Internal Frictional Resistance in the Annular Gap during the Plunger Gas Lift Process. *Processes* **2023**, *11*, 3246. <https://doi.org/10.3390/pr11113246>

Academic Editors: Guoheng Liu, Jianhua Zhao, Xiaolong Sun and Yuqi Wu

Received: 26 October 2023

Revised: 6 November 2023

Accepted: 15 November 2023

Published: 17 November 2023



**Copyright:** © 2023 by the authors. Licensee MDPI, Basel, Switzerland. This article is an open access article distributed under the terms and conditions of the Creative Commons Attribution (CC BY) license (<https://creativecommons.org/licenses/by/4.0/>).

## 1. Introduction

In the process of the continuous extraction of natural gas, a reservoir produces a significant amount of formation water. In the early stage of extraction, when the gas–liquid ratio is relatively high, the high-velocity gas flow carries a large volume of liquid to the wellhead. However, as the reservoir pressure decreases, the gas supply capacity of the formation weakens, and the ability of the gas to carry liquid also diminishes. When the gas-phase flow rate is significantly lower than the critical flow rate, the gas is not able to continuously carry the liquid out of the wellhead, resulting in liquid backflow to the bottom of the well, forming bottomhole fluid accumulation and increasing bottomhole backpressure, which in turn leads to a decline in gas well production [1]. When the bottomhole liquid accumulation reaches a certain level, the bottomhole pressure may exceed the reservoir pressure, leading to a complete shutdown of the gas well, which significantly impacts production operations.

To address this challenge, plunger lift technology, as an economically efficient method for liquid removal and gas extraction, is widely used in oil and gas fields both domestically and internationally. The main principle of this technology is to place a solid plunger in the tubing that can freely move upward and downward to form a solid interface between the gas–liquid two phases. The plunger utilizes the expansion capability of the gas itself to drive its upward movement, serving as a separator between the gas and liquid, effectively

preventing the gas from escaping in the upward direction and the liquid from flowing back and simultaneously eliminating the accumulation of fluid at the bottom of the well [2]. Compared with traditional artificial lifting methods (e.g., mechanical oil recovery, foam drainage, and continuous tubing drainage), plunger gas lift technology does not require additional energy, does not use chemicals, and has the advantages of low cost, low energy consumption levels, and environmental protection [3]. In addition, the plunger can also remove the scale and wax on the inner wall of the tubing and play a role in preventing wax and scale.

In recent years, the research on plunger lift technology mainly focused on the qualitative analysis of experimental patterns and the theoretical modeling of their dynamic characteristics. Representative works include Foss's and Gaul's [4] and others, in 1960, who established a mechanical analysis method of the plunger lift based on the relationship between oil pressure at the wellhead, casing pressure, and production. They proposed a static plunger lift model and presented a version of the plunger lift's operation. In 1982, Lea [5] proposed a transient kinetic model for the plunger by assuming that the plunger and liquid elevated at the same upward velocity. In 1985, Mower [6] presented the empirical relationships between gas slip and liquid leakage and plunger movement velocity by experimental studies, and corrected Foss's and Gaul's static model. His study showed that gas slip decreased with an increasing plunger velocity, while liquid leakage increased with an increasing plunger velocity. Neil Longfellow [7] and others used numerical methods to study plunger lift behavior in horizontal wells and obtained the distribution of pressure and fluid velocities in the annular gap between the channelized plunger and wellbore. Parsa [8] studied the influence of reservoir pressure and other factors on plunger lift behavior, realized the accurate calculation of the gas volume in the lower part of the plunger, and proposed an optimization method for the dynamic model of a plunger lift.

Although the plunger is placed in an annular gap with the tubing as it travels upstream and creates a turbulent seal [9,10] that prevents some of the fluid from falling back down to the bottom of the well, there is still friction generated by the annular gap between the plunger and tubing in the process; since the velocity of the plunger movement in a vertical wellbore can change from moment to moment, it causes the annular gap frictional resistance to change throughout the plunger's upward travel. However, previous studies usually ignored the friction between the plunger and liquid, treating the plunger and liquid column as a single unit and considering only the friction of the liquid column. Therefore, studying the variation in the annular gap frictional resistance between the plunger and tubing remains of significant importance for optimizing plunger lift technology for liquid removal and gas extraction. It provides a theoretical foundation for system optimization and process improvement. These studies have helped to improve oil and gas recovery and promote the sustainable development of the oil and gas industry.

## 2. Experimental Procedure and Equipment

The wellbore consisted of 2 10 m-long acrylic pipes and a 10 m-long steel pipe, with an inner diameter of 62 mm and a wall thickness of 10 mm. This setup was designed to simulate the plunger lift process and observe the motion of the plunger and liquid. A schematic of the device is shown in Figures 1–3. Movable sliders were installed at the top of the experimental setup and interconnected with the vertical steel frame. There was a removable kit supported by sliding brackets to ensure that the pipe could be placed at any angle between 0° and 90°. This ability to adjust the angle was critical for modeling the multiphase flow conditions at different slopes or horizontal positions of the pipe. The main objective of this experimental setup was to study the interaction of gases and liquids under a multiphase pipe flow. By adjusting the angle of the pipe and other parameters, the researchers were able to simulate the plunger lift capacity under different conditions, which was important for understanding the plunger lift motion.

During the experiment, high-pressure compressed air was supplied by an air compressor and stored in a gas storage tank. This high-pressure air was then passed through

a drying chamber that dried the gas. The flow rate of the gas was controlled by a valve downstream of the drying box. The gas flow rate was measured by an orifice plate gas flow meter with a range of 0~200 m<sup>3</sup>/h and an accuracy of ±1%. Meanwhile, water was supplied by a pump and metered by a turbine flow meter at a range of 0~0.3 m<sup>3</sup>/h and accuracy of ±0.3%. High-pressure compressed air and water were thoroughly mixed in the mixer to form a mixed air–water fluid medium, which then entered the test section. At the end of the experiment, water was recovered and air was vented through a gas–liquid separation device attached to the outlet of the test tube section.

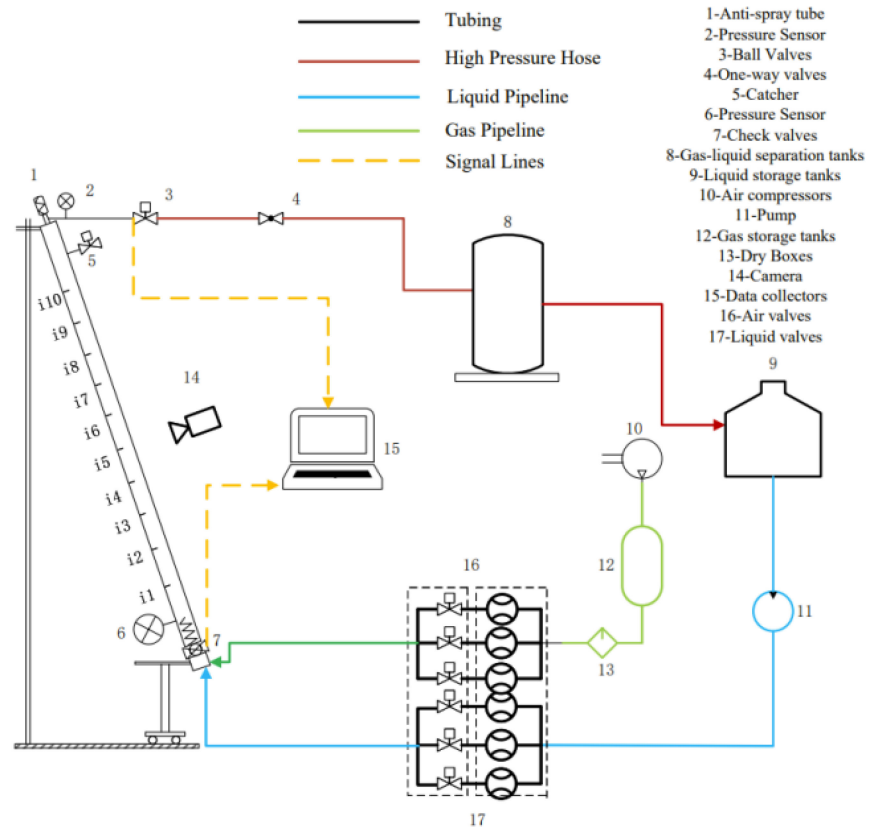
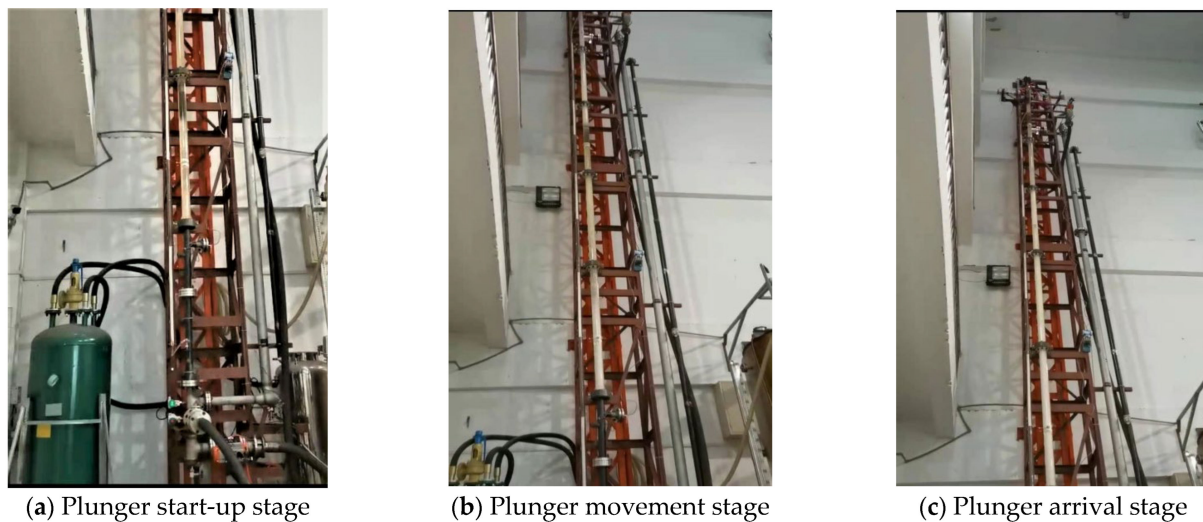


Figure 1. Schematic route of the experimental setup.



Figure 2. Physical diagram of the experimental device.



**Figure 3.** Plunger upward motion process in plunger experiment.

To better observe and understand the plunger airlift process, two pressure sensors were installed in the experiment, located at the inlet and outlet of the pipe. The volume retention of liquids was also measured using snap shut valves, which were located at the inlet and outlet of the pipeline. A high-speed camera was also installed to record the movement of the plunger. All data were uploaded via sensors to a computer terminal for paperless recording and analysis. The design of this experimental setup and data acquisition system allowed the researchers to study the plunger gas lift process in detail, including the flow behavior of the gases and liquids and pressure changes. These data are critical to understanding the characteristics and performance of the gas–liquid two-phase flow, and see Table 1 for relevant parameters.

**Table 1.** Measuring range and accuracy of measuring equipment.

Measurement Equipment	Measurement Range	Measurement Precision (%)
Gas flow meter	34.72 m <sup>3</sup> /min	±1
Liquid flow meter	0–20 m <sup>3</sup> /h	±0.3
Differential pressure sensor	–10–100 KPa	0.025–0.04
Pressure transmitter	0–5 MPa	±0.5
Temperature sensor	0~90 °C	±1

To achieve accurate instantaneous velocity measurements, self-developed geomagnetic sensors were used in the study, which were arranged at different locations on the pipe section, as shown in Figure 1, from i1 to i10. These geomagnetic sensors were able to instantly detect changes in the magnetic field inside the pipe column, and when the magnetic field changed, their frictional resistance characteristics changed accordingly and then transmitted this information in the form of electrical signals to the data acquisition port and converted it into digital signals. This geomagnetic sensor application allowed the researchers to obtain precise instantaneous velocity data of the plunger in the experiments without relying on traditional mechanical or optical measurement methods. By monitoring the changes in the magnetic field, these sensors were able to provide high-resolution and high-accuracy velocity measurements, providing a more complete understanding of the plunger’s kinematic behavior and providing an accurate database for the research. This is valuable for analyzing the gas–liquid two-phase flow characteristics in plunger lift studies.

### 3. Experimental Results and Analysis

#### 3.1. Plunger Movement Analysis

In the in-house simulation experiment, we took some pictures of the turbulent seal in the plunger recess during the upward travel of the plunger.

The results obtained by most scholars through numerical simulations are in line with our study, i.e., a turbulent sealing effect occurs in the grooves, as shown in Figure 4, which reduces the tendency of the liquid to fall back to a large extent. However, through a careful analysis of the actual data, we found that the movement of the plunger was greater than that of the liquid column, which was the main cause of the liquid fallback. The presence of this velocity difference could not be ignored. In addition, this fallback phenomenon could not simply be attributed to liquid slippage or the self-weight of the liquid. Since the plunger traverses the liquid column to trigger a high volume of liquid leakage, this paper suggests that a certain level of frictional resistance is also generated within the annular gap between the plunger and tubing. Therefore, when calculating the frictional resistance, the effects of the frictional resistance within the annular gap could not simply be treated together, but they needed to be calculated and analyzed separately.

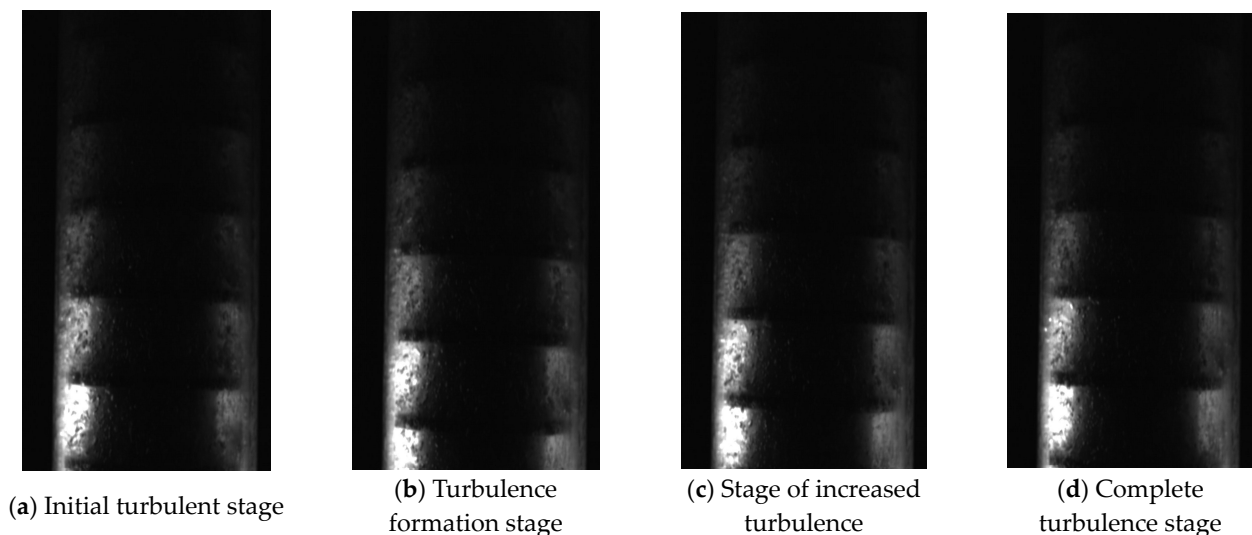


**Figure 4.** The fluid flow state inside the grooves of a rod-type plunger in a plunger lift system.

Some examples of the relevant data are shown below, Table 2.

**Table 2.** Relative differential velocity values for plunger and liquid columns.

$P_{wf}$ (KPa)	$P_c$ (KPa)	$P_t$ (KPa)	Average Velocity	Liquid Column Movement Speed	Plunger Movement Speed	Relative Speed
219	171	161	4.80	4.83	5.00	0.17
214	159	158	5.01	5.00	5.38	0.38
205	151	148	4.34	4.83	5.00	0.17
202	150	146	5.54	4.24	5.83	1.59
202	147	141	4.74	4.38	5.60	1.23
202	150	144	4.34	3.78	5.19	1.40
211	159	151	5.95	4.52	5.60	1.08
202	150	144	5.63	4.52	5.19	0.67
252	201	189	5.34	4.83	5.60	0.77
255	200	193	5.86	5.19	6.67	1.48
264	212	186	5.63	5.19	6.09	0.90
270	215	198	5.89	5.19	6.67	1.48
270	216	199	6.05	5.38	6.67	1.28
252	201	193	4.47	6.09	8.24	2.15

Table 2. Cont.

$P_{wf}$ (KPa)	$P_c$ (KPa)	$P_t$ (KPa)	Average Velocity	Liquid Column Movement Speed	Plunger Movement Speed	Relative Speed
257	197	190	6.15	4.12	5.83	1.72
261	201	196	5.63	5.00	6.09	1.09
255	198	192	5.81	5.00	6.36	1.36
317	256	256	5.15	6.09	7.00	0.91
308	251	244	7.11	5.60	7.37	1.77
302	241	242	6.45	5.38	6.67	1.28
313	257	245	7.05	6.09	7.37	1.28
305	251	239	6.61	5.19	7.00	1.81
313	257	251	6.81	6.09	7.00	0.91
305	242	235	5.81	5.00	6.67	1.67
307	247	242	4.93	5.00	6.67	1.67
310	248	245	5.76	5.00	7.00	2.00

These data provide the reason for the experimentally observed velocity differences between the plunger and liquid column, and the frictional resistance generated within the annular gap could not be ignored. This helped to provide a further understanding of the various influences on the plunger lift process, including velocity differences and frictional resistance, thus providing a more accurate basis for our analysis. These results are important for optimizing the gas lift process and system design.

### 3.2. Analysis of Frictional Resistance in the Plunger Annular Gap

The goal of a plunger lift is to lift as much liquid as possible while using the least amount of energy. During the gas lift process, the inner wall annular gap can lead to liquid leakage and gas slip phenomena. The ascent of the plunger is a complex process involving the motion of the plunger and the exchange of mass and momentum between the gas and liquid through the annular gap. To better analyze the internal friction of the fluid in the annular gap, we modeled the forces in the annular gap. The physical model of the plunger lift is shown in Figure 5, which includes the liquid-phase region in the upper part of the plunger, the gas-phase region in the lower part of the plunger, and the turbulent region of the gas–liquid phases in the annulus of the plunger. This model helps us gain a deeper understanding of the interactions between different regions during the plunger lift process, especially the flow of the liquid within the annular gap and the upward movement of gas. By analyzing the model, we can optimize the plunger lift technology more effectively, reduce energy consumption levels, and enhance liquid collection efficiency.

Consider the fluid in the upper part of the plunger and the plunger as a single unit, assuming that it is moving upward with velocity. In this case, the main forces exerted include:

1. Plunger upper surface pressure: the hydrostatic pressure of the liquid and the hydrostatic column pressure on the top of the plunger due to the liquid above the plunger,  $\pi d^2 p_1 / 4$ .
2. Plunger lower surface pressure: at the bottom of the plunger, the dynamic column pressure from the annulus and formation is applied,  $\pi d^2 p_2 / 4$ .
3. Gravity of the plunger and liquid column: since both the plunger and liquid column have a certain mass, they are subject to a constant force of gravity,  $(m_p + m_l)g$ .
4. Frictional resistance of the liquid column and inner wall of the tubing: when the liquid column moves upward with the plunger, the friction between the liquid and inner wall of the tubing hinders the upward movement of the plunger,  $F_{f1}$ .
5. Fluid friction in the annular gap: since gases and liquids move turbulently in the annular gap and move upward with the plunger, the friction in the annular gap also affects the plunger's movement,  $F_{f2}$ .

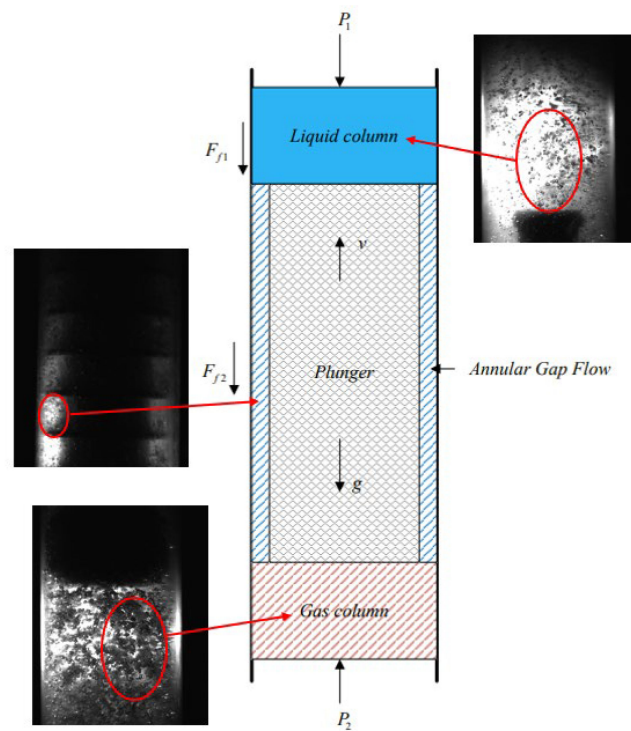


**Figure 5.** Schematic diagram of the physical model for the plunger lift.

These forces determine the ascent velocity of the plunger and the extent of liquid leakage during the plunger lift process. By analyzing the effects of these forces, we can gain a better understanding of the plunger lift process and conduct corresponding process optimizations to improve the efficiency.

The force expression for plunger and liquid column lifting is as follows:

$$(m_l + m_p)a = \pi d^2(P_2 - P_1)/4 - (F_{f1} + F_{f2}) - (m_l + m_p)g \quad (1)$$

where  $m_l$  and  $m_p$  are the mass values of the plunger and liquid column, respectively, kg;  $a$  is the upward acceleration of the plunger,  $m/s^2$ ;  $d$  is the inner diameter of the tubing, m;  $P_1$  and  $P_2$  are the pressure levels on the upper and lower surfaces of the plunger, respectively, Pa; and  $g$  is the acceleration of gravity,  $m/s^2$ .

The friction ( $F_{f2}$ ) between the annular fluid and inner wall surface of the tubing can be solved by the calculation method above.

By the concept of equivalent radius, for the annular gap space flow, there is:

$$d_{eff} = \frac{4 \times \frac{\pi}{4}(d_2^2 - d_1^2)}{\pi(d_2 + d_1)} = d_2 - d_1 \quad (2)$$

The frictional-resistance coefficient ( $f_2$ ) of the ring seam can be calculated from the experimental data by Equation (3):

$$F_{f2} = \frac{f_2 \rho_l A_{eff} H_p v^2}{2d_{eff}} \quad (3)$$

Some of the frictional-resistance coefficient data are shown below, Table 3.

**Table 3.** Partial frictional-resistance coefficient data.

Bottomhole Pressure (KPa)	Casing Pressure (KPa)	Tubing Pressure (KPa)	Speed of Movement (m/s)	Annular Gap Friction (N)	Annular Gap Friction Factor
202	148	138	5.11	4.977153	0.06751
204	156	146	5.71	6.383483	0.06914
205	157	144	5.86	6.473506	0.06671
204	153	141	5.15	5.128638	0.06838
204	160	143	5.29	5.1804	0.06556
205	160	146	5.11	5.307037	0.07198
204	150	144	5.06	4.724593	0.06536
204	150	144	5.11	5.195129	0.07047
205	150	140	5.29	5.46595	0.06897

To better describe this dynamic trend, we needed to introduce another dimensionless variable to characterize the change in the coefficient of frictional resistance. In the same treatment as before, we established a plot between the Reynolds number and coefficient of frictional resistance, where the Reynolds number was calculated as follows:

$$Re = \frac{\rho v d_{eff}}{\mu} \quad (4)$$

In the formula,  $Re$  represents the Reynolds number, dimensionless;  $v$  is the fluid velocity, m/s;  $d$  is the equivalent inner diameter, m;  $\rho$  is the fluid density, kg/m<sup>3</sup>; and  $\mu$  is the dynamic viscosity of the fluid, m<sup>2</sup>/s, with an experimental water dynamic viscosity of 10<sup>-6</sup> m<sup>2</sup>/s used for the calculation.

The relationship graph (Figure 6) between the Reynolds number and frictional-resistance coefficient assisted us in gaining a more comprehensive understanding of how the frictional-resistance changed with variations in the Reynolds number. This, in turn, aided us in optimizing the design and operation of plunger lift processes.

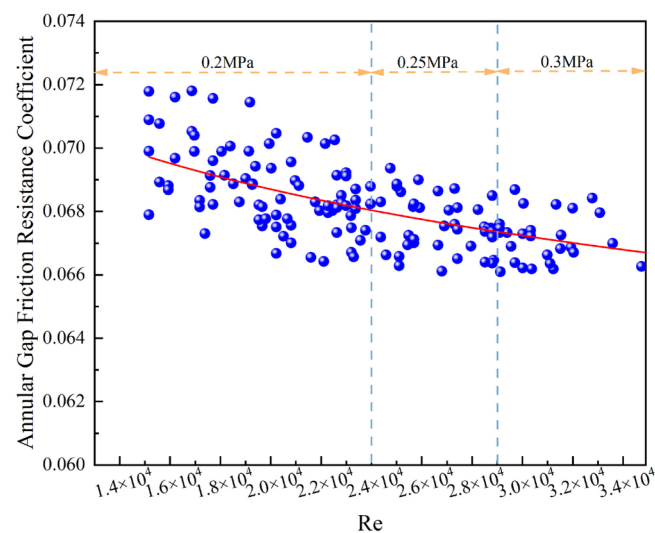


**Figure 6.** Plot of plunger annular gap friction coefficient results (The blue dots represent experimental data points and the red line represents the data trend line).

The upward movement velocities of the plunger at 0.2 MPa, 0.25 MPa, and 0.3 MPa were tested in a Plexiglas tube by indoor plunger lift experiments and analyzed computationally, and the results are shown in Figure 6. The Reynolds number interval under 0.2 MPa was mainly concentrated at  $1.4 \times 10^4 \sim 2.4 \times 10^4$ , and its annular gap frictional-resistance coefficient was mainly concentrated at 0.066~0.072. The Reynolds number

interval at 0.25 MPa was mainly concentrated at  $2.4 \times 10^4 \sim 2.9 \times 10^4$  and its annular gap frictional-resistance coefficient was mainly concentrated at 0.066~0.070. The Reynolds number interval at 0.3 MPa was mainly concentrated in the range of  $2.9 \times 10^4 \sim 3.4 \times 10^4$  and its annular gap frictional-resistance coefficient was mainly concentrated in the range of 0.066~0.069.

Overall, the dynamic trends were manifested in the following ways: the annular gap frictional-resistance coefficient decreased sharply in the interval from  $1.4 \times 10^4$  to  $2.4 \times 10^4$ ; in the interval of  $2.4 \times 10^4 \sim 2.9 \times 10^4$ , the decrease in the annular gap frictional-resistance coefficient gradually slowed down and showed an excessive value; and in the interval of  $2.9 \times 10^4 \sim 3.4 \times 10^4$ , the annular gap tended to flatten out, showing a steady state. The overall trend was a gradual shift from a rapid decline to a constant smoothness.

Meanwhile, we conducted a statistical test and found that the correlation coefficient was  $-0.7252$ , which corresponded to a  $p$ -value of  $7.42 \times 10^{-20}$ . Therefore, we rejected the 0 hypothesis (the regression coefficient was not significant) and accepted the alternative hypothesis (the regression coefficient was significant).

### 3.3. Comparative Analysis of Different Frictional-Resistance Coefficient Formulas

For the calculation of the coefficient of friction, the formula method and Moody resistance diagram method are usually used as the two most common methods. The formulaic methods used at present include Moody’s [11], Wood’s [12], Jain’s [13], Churchill’s [14], and Chen’s [15] formulas. The five commonly used models and, Re ranges and relative roughness ranges are shown in Table 4.

**Table 4.** Different frictional-resistance coefficient models and their scopes of application.

Name	Model	Re Adaptation Range	$\epsilon/d$ Range of Adaptation
Moody	$f_D = 5.5 \times 10^{-3} [1 + (2 \times 10^4 \epsilon/D + 10^6 / \text{Re})^{1/3}]$	$[4 \times 10^3, 10^7]$	$[1 \times 10^{-5}, 0.05]$
Wood	$f_D = 0.094 (\frac{\epsilon}{D})^{0.225} + 0.53 (\frac{\epsilon}{D}) + 88 (\frac{\epsilon}{D})^{0.4} (\text{Re})^{-1.62} (\frac{\epsilon}{D})^{0.134}$	$[4 \times 10^3, 10^7]$	$[4 \times 10^{-5}, 0.05]$
Jain	$\frac{1}{\sqrt{f_D}} = 1.14 - 2 \log (\frac{\epsilon}{D} + \frac{21.25}{\text{Re}^{0.9}})$	$[5 \times 10^3, 10^7]$	$[4 \times 10^{-5}, 0.05]$
Churchill	$f_D = 8 [(\frac{8}{\text{Re}})^{12} + \frac{1}{(A+B)^{3/2}}]^{1/12}$ $A = \{2.457 \ln[(\frac{7}{\text{Re}})^{0.9} + 0.27 \frac{\epsilon}{D}]\}^{16}$ $B = (\frac{37530}{\text{Re}})^{16}$	All scopes	All scopes
Chen	$f_D = -2.0 \log [\frac{\epsilon/D}{3.7065} - \frac{5.0452}{\text{Re}} \log (\frac{(\epsilon/D)^{1.1098}}{2.8257} + \frac{5.8506}{\text{Re}^{0.8981}})]$	$[4 \times 10^3, 4 \times 10^8]$	$[5 \times 10^{-7}, 0.05]$

By substituting the corresponding Reynolds numbers, equivalent diameters, and relative roughness ( $\Delta 0.15$  mm) into the abovementioned five friction coefficient calculation formulas, we could obtain the friction coefficients at different Reynolds numbers for these five cases, as shown in Figure 7.

From Figure 7, it can be clearly observed that in the same range of the Reynolds numbers, all the five models used for the calculation of the friction coefficients show a decreasing friction coefficient trend with an increasing Reynolds number, which is consistent with our expected results [16–27]. However, by comparing the results of these computational models with the experimental data, we found the following range of variation in the coefficient of friction: the Moody formula had a range of 0.04995 to 0.05106 for the coefficient of friction, with a decrease of 0.00111; Wood’s formula had a resistance coefficient interval of 0.054239 to 0.054241, with a decrease of  $1.0 \times 10^{-6}$ ; Jain’s and Churchill’s formulas had resistance coefficients in the range of 0.05445 to 0.05544, with a decrease of 0.00216; and Chen’s formula had resistance coefficients in the range of 0.054 to 0.05535, with a decrease of 0.00135. Compared to the magnitude of the decrease in these computational models, the experimental data have a range of friction coefficients between 0.0651 and 0.072. These computational models have a relatively smooth variation in the friction coefficient. However, by comparing the absolute errors of the results of these computational models

with the experimental data, we obtained the following absolute errors: 25.99%, 20.31%, 19.09%, 18.99%, and 19.91%. These results show that none of the abovementioned five models used for calculating the frictional-resistance coefficient can accurately reflect the plunger annular gap frictional-resistance coefficient, as shown in Figure 8.

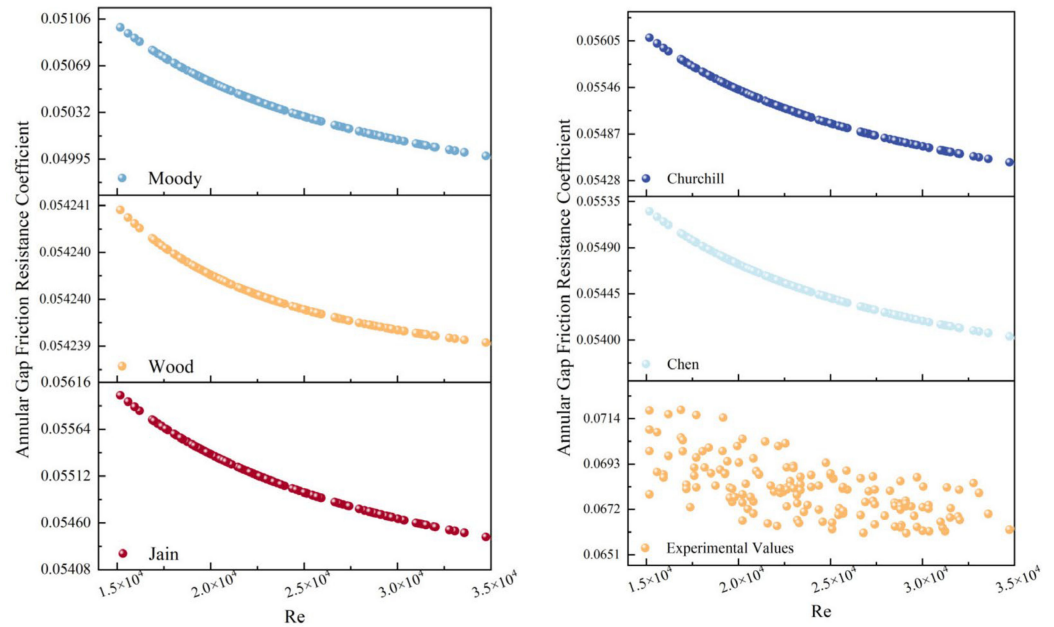


**Figure 7.** Comparison of calculated and experimental values of different frictional-resistance coefficient models.

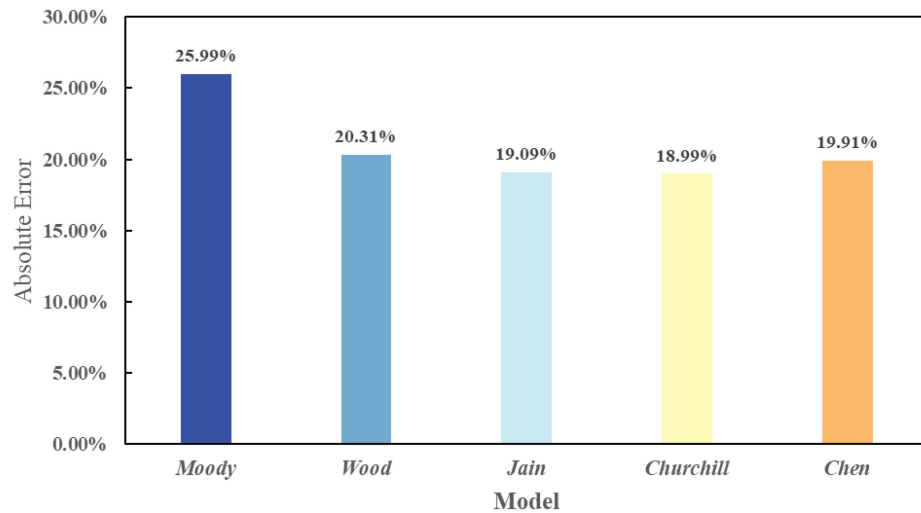


**Figure 8.** Comparison of absolute errors of different models for calculation of friction coefficients.

Upon further analyses, we believed that, in this scenario, the frictional force within the annular gap was primarily generated by the turbulent state created by the plunger interacting with the liquid inside the annular gap. Additionally, on one side close to the pipe wall, there existed a liquid film that interacted with the pipe wall through friction, as illustrated in Figure 9. The frictional forces at different interfaces collectively contributed to the overall annular gap frictional resistance. In addition, as evidenced by the phenomena observed in Section 3.1, there was a discrepancy between the speed of movement of the plunger and the speed of movement of the liquid column, resulting in a significant amount of liquid leakage.

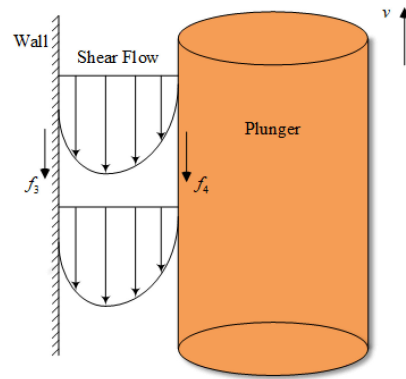


Figure 9. Schematic representation of friction in the annular gap.

Therefore, this study concludes that, in this case, the five commonly used friction coefficient models mentioned above are difficult to apply to the flow situation inside the annular gap and, therefore, a model for calculating the friction coefficient adapted to this condition is needed.

#### 4. Modeling of Annular Gap Frictional-Resistance Coefficient

Find the distribution of the flow velocity near the wall according to Plante’s hypothesis of  $l = ky$ . The associated solution is presented below:

$$\rho k^2 y^2 \left| \frac{d\bar{u}}{dy} \right| \frac{d\bar{u}}{dy} = \tau_0 \tag{5}$$

For a positive value of  $\frac{d\bar{u}}{dy}$ ,  $\left| \frac{d\bar{u}}{dy} \right| = \frac{d\bar{u}}{dy}$ , obtain:

$$u_* = \sqrt{\frac{\tau_0}{\rho}} \tag{6}$$

where  $u_*$  is the shear stress velocity, which can be expressed as:

$$\frac{1}{u_*} \frac{d\bar{u}}{dy} = \frac{1}{ky} \tag{7}$$

Points scored:

$$\frac{u}{u_*} = \frac{1}{k} \ln y + C \tag{8}$$

Taking the flow velocity at thickness  $\delta$  of the near-wall flow layer  $u_0$  as in Figure 10, there are:

$$\frac{u_0}{u_*} = \frac{1}{k} \ln \delta + C \tag{9}$$

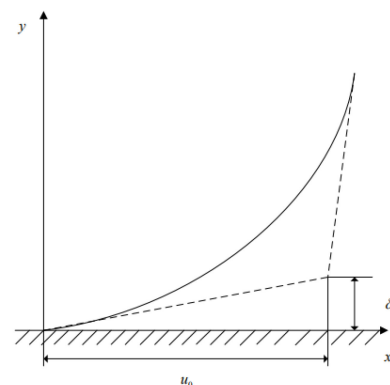


Figure 10. Near-wall flow velocity.

To determine  $u_0$ , it is understood from Equation  $\bar{u} = \frac{\tau_0}{\mu}y$  that  $\bar{u} = u_0$  when  $y = \delta$ :

$$\tau_0 = \mu \frac{u_0}{\delta} \quad (10)$$

From the equation above, we achieve:

$$u_0 = \tau_0 \frac{\delta}{\mu} = \rho u_*^2 \frac{\delta}{\mu} \quad (11)$$

As a result:

$$\frac{u_0}{u_*} = \frac{\rho u_* \delta}{\mu} = N \quad (12)$$

Then, from Equation (9):

$$C = \frac{u_0}{u_*} - \frac{1}{k} \ln \delta = N_* - \frac{1}{k} \ln \left( \frac{N_* \mu}{\rho u_*} \right) \quad (13)$$

Substituting this into Equation (8) provides the turbulent zone flow velocity distribution:

$$\frac{\bar{u}}{u_*} = \frac{1}{k} \ln y + N_* - \frac{1}{k} \ln \left( \frac{N_* \mu}{\rho u_*} \right) = N_* - \frac{\ln N_*}{k} + \frac{1}{k} \ln \left( \frac{\rho u_* y}{\mu} \right) = G + \frac{1}{k} \ln \left( \frac{\rho u_* y}{\mu} \right) \quad (14)$$

Substituting this into Equation (8) produces the turbulent zone flow velocity distribution:

$$\frac{\bar{u}}{u_*} = 1.95 + 2 \ln \left( \frac{\rho u_* y}{\mu} \right) \quad (15)$$

In practice, we were most interested in the section-averaged flow rate  $v$  rather than the time-averaged point velocity  $\bar{u}$ , for which  $\bar{u}$  needed to be converted into  $v$ . The average flow rate of the section-averaged point velocity  $v$ - was the average flow rate of the section-averaged point velocity.

$$v = \frac{Q}{A} = \frac{1}{\pi r_0} \int_0^{r_0} \bar{u} 2\pi(r_0 - y) dy \quad (16)$$

For rough tubes, substituting  $\bar{u}$  from Equation (15) into Equation (16) yields:

$$\frac{v}{u_*} = 13.37 + 2 \ln \left( \frac{r_0}{\delta} \right) \quad (17)$$

The flow velocity distribution of the hydraulic rough tube (Equation (17)) is presented in the above equation:

$$\lambda = \frac{2gdh_f}{Lv^2} = \frac{2gd\Delta p}{\gamma Lv^2} = \frac{2d\Delta p}{\rho Lv^2} \quad (18)$$

This is converted again into:

$$\tau_0 = -\frac{r_0}{2} \frac{\partial p}{\partial x} = \frac{d}{4} \frac{\Delta p}{L} \quad (19)$$

Eliminating  $\Delta p$ ,  $L$ , and  $d$  from the two equations above, we obtain:

$$\lambda = \frac{8\tau_0}{\rho v^2} = \frac{8u_*^2}{v^2} \quad (20)$$

where  $\tau_0 = \rho u_*^2$ , and thus:

$$\frac{v}{u_*} = \sqrt{\frac{8}{\lambda}} \quad (21)$$

Substituting Equation (21) into Equations (15) and (17), eliminating  $u_*$ , and taking  $Re = \frac{\rho v D_{eff}}{\mu}$  into account, we can obtain the formula for the coefficient of the along-stroke resistance  $\lambda$  of the liquid between the plunger and gap:

$$\frac{1}{\sqrt{f_D}} = 1.246 - 2 \log_{10} \left( \frac{\varepsilon}{d_{eff}} + \frac{1.376}{Re^{0.45}} \right) \quad (22)$$

In the equation,  $\Delta$  is the absolute roughness value, mm;  $d_{eff}$  is the equivalent radius, mm;  $Re$  is the Reynolds number;  $\rho$  is the fluid density,  $\text{kg}/\text{m}^3$ ;  $v$  is the plunger's velocity,  $\text{m}/\text{s}$ ;  $D_{eff}$  is the equivalent diameter, m; and  $\mu$  is the fluid dynamic viscosity,  $\text{kg}/(\text{m}\cdot\text{s})$ .

By substituting the Reynolds number and corresponding relative roughness at different speeds into Equation (22), the corresponding coefficient of frictional resistance can be calculated. Subsequently, the calculated and experimental values are plotted in the same graph as shown in Figure 11.

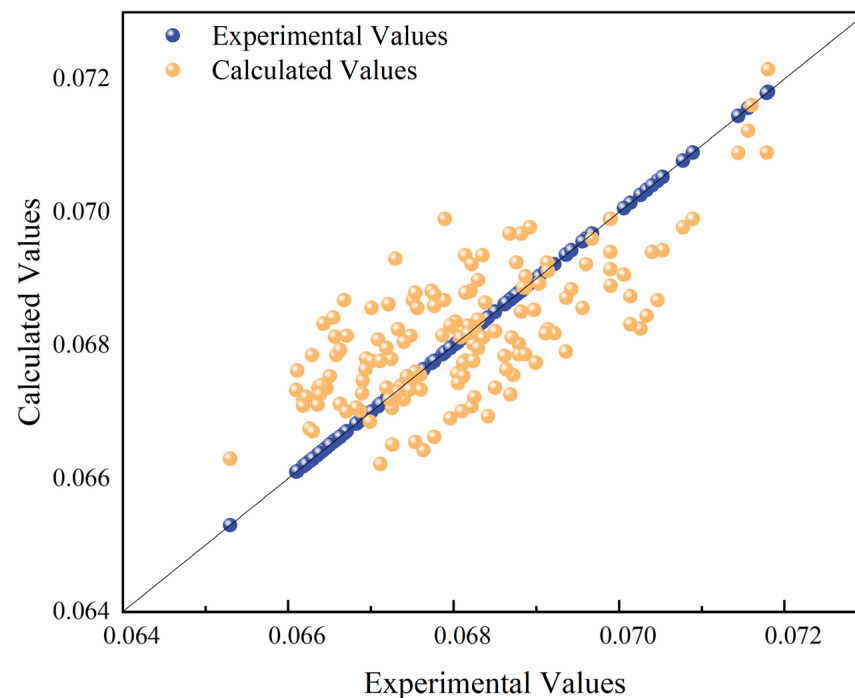


**Figure 11.** Comparison between experimental and calculated values of annular gap frictional-resistance coefficients.

The calculation results in Figure 12 show that the overall trend of the drag coefficient calculation model is to decrease with an increasing Reynolds number under vertical well-bore conditions, showing a negative correlation. Compared to the five commonly used friction coefficient calculation models, this model is more in line with the calculation of the annular gap friction coefficient in plunger lift operations. In addition, a relative error analysis was performed with an error of  $\pm 4\%$  and a residual sum of 0.22. This indicates that, under specific flow conditions, our friction coefficient calculation model can more accurately reflect the frictional resistance within the annular gap, providing a more reliable theoretical basis for plunger lift technology.

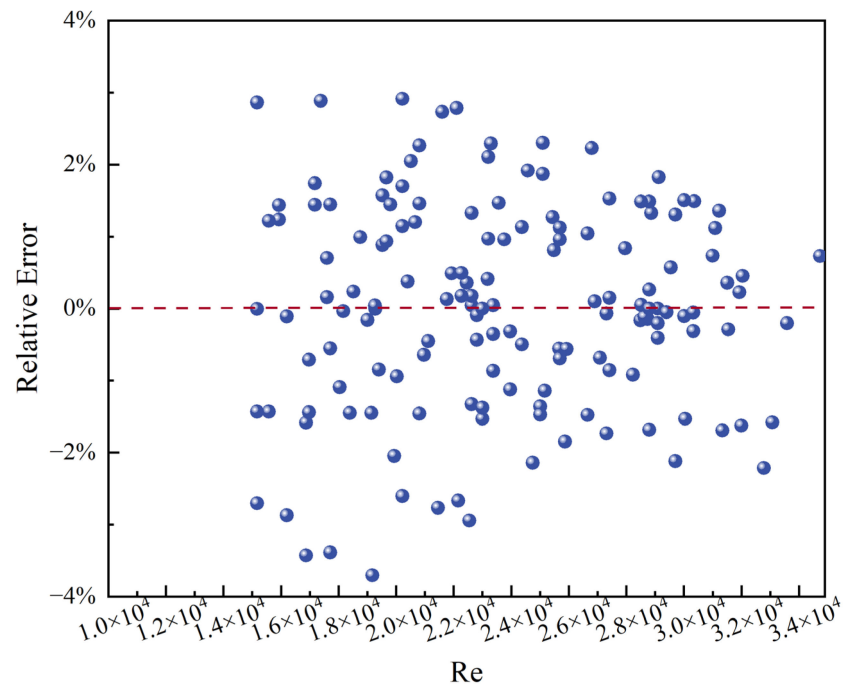


**Figure 12.** Comparison of relative errors between calculated and experimental values (The blue dots represent the relative error between the experimental and predicted values).

In this paper, error calculations, such as the coefficient of determination ( $R^2$ ), mean absolute percentage error (MAPE), and root mean square error (RMSE), were used for the model comparison. Where the RMSE was used to measure the deviation between the predicted and experimental values, the smaller the error was, the better the predictive ability of the model. These error calculation methods can help us evaluate the performance of each model to determine that model that is more suitable for describing the trend of the resistance coefficient of the annular gap in the plunger lift.  $R^2$ , MAPE, and RMSE values are calculated as follows:

$$R^2 = 1 - \frac{\sum_i (\hat{y}_{cal} - y_{exp})^2}{\sum_i (\hat{y}_{exp} - y_{cal})^2} \quad (23)$$

$$MAPE = \left( \frac{1}{n} \sum_1^n \left| \frac{f_{cal} - f_{exp}}{f_{exp}} \right| \right) \times 100\% \quad (24)$$

$$RMSE = \sqrt{\sum_{i=1}^n (\hat{y}_{cal} - y_{exp}) / n} \quad (25)$$

where  $f_{cal}$  is the model predicted value of the plunger annulus-resistance coefficient,  $f_{exp}$  is the experimental value of the plunger annulus-resistance coefficient.

From the RMSE prediction evaluation results presented in Table 5, it can be seen that the Churchill prediction model provides the most accurate prediction among the five models, with a difference in the root mean square error of approximately 1.29. The Moody prediction model predicts a large bias with a root mean square error of 1.77. The remaining three models are basically in the middle of the error range of approximately 1.35. The new model proposed in this paper presented the smallest error, with an RMSE of 0.39 and a mean absolute percentage error of 2.20%. These results indicate that the new model proposed in this paper exhibits greater accuracy and reliability in predicting the variation trend of the frictional-resistance coefficient within the annular gap in plunger lift technology.

**Table 5.** Calculation error of the frictional-resistance coefficients for different plunger annular gaps.

Model Name	R <sup>2</sup>	MAPE	RMSE
Moody	0.051	25.99%	1.77
Wood	0.088	20.31%	1.39
Jain	0.089	19.09%	1.31
Churchill	0.089	18.99%	1.29
Chen	0.085	19.91%	1.36
Article	0.74	2.20%	0.39
Mean Experimental Value	0.06809	Mean Predicted Value	0.06810

## 5. Case Study

Known as the 1# gas well in southern Sichuan, China, the well has a measured depth of 5270 m, a vertical depth of 3572.8 m, and a caliper vertical depth of 3500 m; the wellhead oil pressure is 10 MPa, wellhead casing pressure is 10 MPa, reservoir pressure is 25 MPa; wellhead temperature is 20 °C, and bottomhole temperature is 60 °C. The inner diameter of the tubing is 0.062 m, the diameter of the plunger is 0.058 mm, the weight of the plunger is 10 kg, and the length is 1 m. The operating schedule shows the well is open for 3 h, then closed for 3 h, with a plunger arrival time of 9 min. In this paper, we considered the existence of annular gap friction on the basis of the original simulation and analyzed it in comparison to other values. The simulation results are shown in Figure 13.

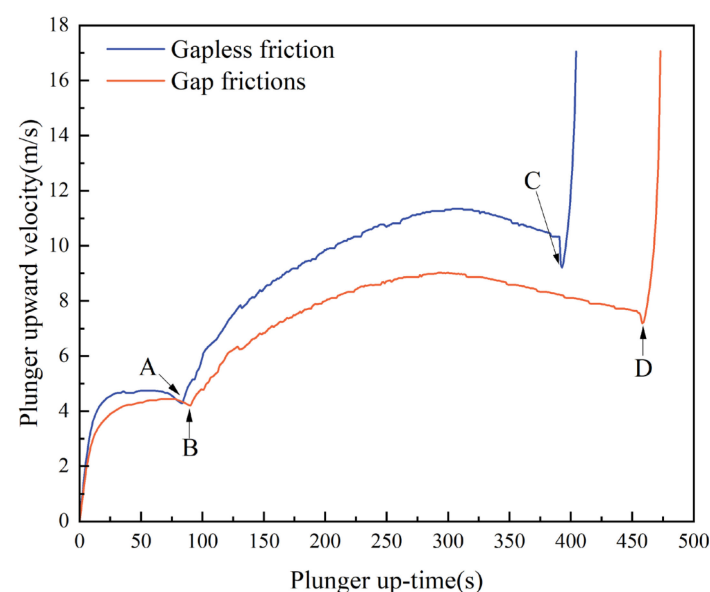


**Figure 13.** Plot of plunger reach time vs. upward velocity (Points A and B in the figure represent the annulus fluid entering the tubing; points C and D in the figure represent the start of fluid discharge from the wellbore).

Based on the analysis of the data in Figure 13, the total upward travel time for the plunger to reach the wellhead without considering the annular gap friction is 404.33 s (i.e., 7 min and 13 s), and the average speed of the plunger's movement is 9.52 m/s. However, when the case of annular gap friction was considered, the time for the plunger to reach the wellhead increased to 472.87 s (i.e., 8 min and 28 s), and the average velocity of the plunger's movement was reduced to 7.78 m/second. By comparing the time difference between the two at 1 min 15 s and the speed difference between the two at 1.73 m/s, the following conclusion can be clearly drawn: the upward travel time of the plunger is closer to the actual travel time of 9 min when considering the annular gap friction between the plunger and pipe wall.

In Figure 13, points A and B represent the turning points of the liquid from the annular space into the tubing when the annular gap frictional resistance is not considered and when the annular gap frictional resistance is considered, respectively. This indicates that, at the same feed rate, the timing of complete fluid entry into the tube is not very different in the two cases. Segment AC represents the start of acceleration of the plunger as the annular air body enters the fuel line when the annular gap frictional resistance is not taken into account. During this time, the acceleration of the plunger is relatively high, with a peak velocity occurring at approximately 310 s. The BD segment represents the scenario when the annular gap frictional resistance is taken into account. When gas from the annular gap enters the tube, the plunger also begins to accelerate. However, as the annular gap frictional resistance is taken into account, the acceleration of the plunger is low, and peak velocity occurs at approximately 300 s. This suggests that the plunger will enter the deceleration phase earlier when considering the annular gap frictional resistance, and therefore the arrival of the fluid from the top of the plunger at the wellhead will be delayed. The CE and DF segments represent the scenarios after the upper liquid is discharged from the wellhead by the plunger. During these two segments, the plunger again enters a phase of accelerated motion due to the reduced pressure at the upper end of the plunger. However, the acceleration is the same in the CE and DF segments, indicating that, in both segments, the fluid on top of the plunger is reduced and the annular gap frictional resistance essentially no longer affects the plunger's speed of motion.

In Figures 14 and 15, the pressure changes on the upper- and lower-end surfaces of the plunger, which are compared with and without considering the annular gap frictional resistance. First, in the upper-end case, since the upper part is only affected by the static gas column pressure, the liquid column pressure, and the wellhead backpressure, there is little difference in the pressure between the two cases, except for the extended time. This is because the upper-end face is primarily affected by the conditions at the wellhead, which are essentially the same in both cases.

Second, in the case of the lower face, when the gas has not yet entered the tubing, there is not much difference in the pressure between the two cases. However, over time, a great difference in pressure began to emerge between the two. This was because, with the annular gap frictional resistance taken into account, the upward velocity of the plunger was reduced, and the fluid was discharged at a slower rate, resulting in a relatively high pressure on the lower face. Without considering the annular gap frictional resistance, the plunger travels upward faster, and the fluid is discharged faster, so the pressure at the lower face is lower.

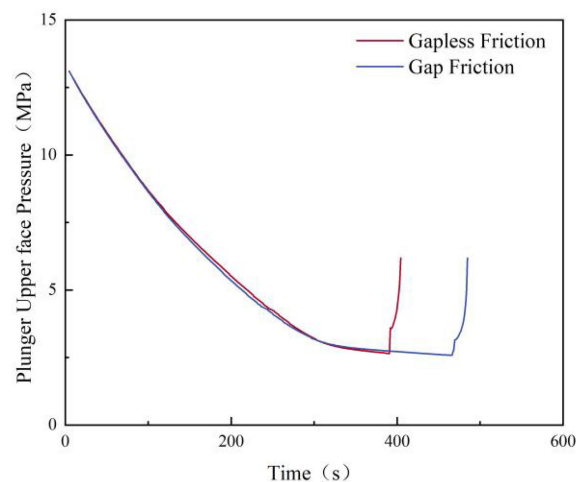


**Figure 14.** Plunger upper-face pressure comparison.

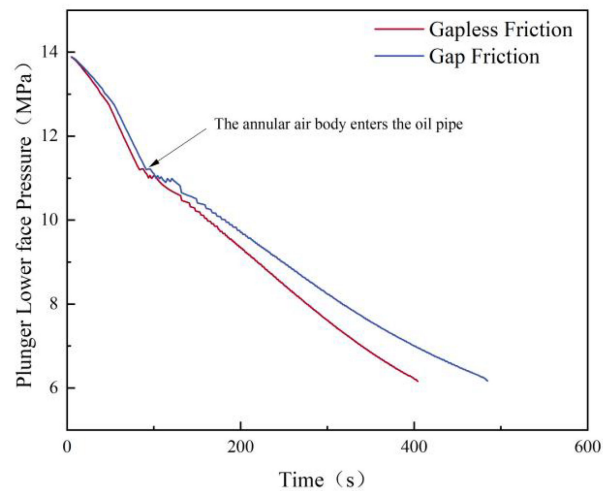


**Figure 15.** Plunger lower-face pressure comparison.

These differences indicate that, with the annular gap frictional resistance taken into account, the liquid is discharged at a slower pace during the upward movement of the plunger, resulting in a relatively high pressure level at the lower-end face, whereas without the annular gap frictional resistance, the liquid is discharged faster and the pressure at the lower-end face is relatively low.

According to Figure 16, the motion acceleration of the plunger with respect to time can be analyzed in detail.

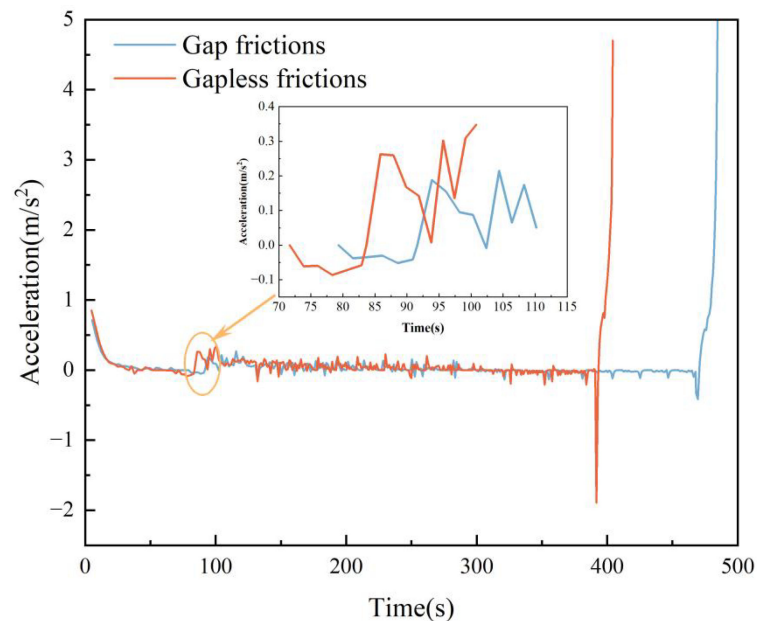


**Figure 16.** Plot of plunger travel time vs. upward acceleration.

At the instant the plunger is released, the plunger gains acceleration for an upward motion. This is because the fluid enters the tube from the annulus and provides the plunger with a short thrust, resulting in a peak acceleration of approximately  $1 \text{ m/s}^2$ . Over time, the plunger gradually reaches dynamic equilibrium, fluid continues to pour into the tube, and the acceleration tends to zero.

As seen in the localized enlargement of Figure 16, at 85 s, the acceleration of the plunger increases again without considering the frictional resistance of the annular gap, with a peak close to  $0.3 \text{ m/s}^2$ , and when the annular gap frictional resistance is considered, the acceleration of the plunger increases again at approximately 95 s, with a peak close to

0.2 m/s<sup>2</sup>. This is because, at this point, the liquid in the annulus has completely entered the tubing, and the subsequent entry is the gas in the annulus.

Over time, the acceleration of the plunger gradually approaches zero and enters a steady phase. Then, it enters a deceleration phase where the acceleration becomes negative. When the liquid column reaches the wellhead and begins to discharge, the liquid column above the plunger decreases, causing the pressure above the plunger to decrease, resulting in a gradual and considerable increase in acceleration. The results of these analyses help to us understand the kinematic characteristics of the plunger, especially the trend of acceleration that affects the ascent of the plunger when considering the frictional resistance of the annular gap.

## 6. Conclusions

With the wide application of the plunger gas lift process, the plunger gas lift shows a good lifting performance, but the frictional resistance in the annular gap is often neglected in real production scenarios. Through indoor experiments, we found that the frictional resistance in the annular gap significantly affected the movement of plunger lifting and derived a model for calculating the coefficient of frictional resistance adapted to the annular gap; the frictional resistance was more accurately calculated through the case study. In detail, the important conclusions of this paper are as follows.

1. In this paper, although the experimental results indicate that the turbulent sealing effect inside the grooves can mitigate the impact of liquid fallback, the analysis of the actual data suggests that the velocity difference between the plunger and liquid column is the primary reason for leakage. This velocity difference cannot be ignored, the leakage phenomenon cannot be simply attributed to fluid slippage or self-weight, and the existence of this velocity difference requires a consideration of the effect of frictional resistance in the annular gap.
2. Through the analysis of the relationship between the Reynolds number and annular gap frictional-resistance coefficient, we found that the annular gap frictional-resistance coefficient showed a decreasing trend with the increase in the Reynolds number. Under different pressure conditions, the changes in the annular gap frictional-resistance coefficient showed a pattern of a rapid decrease, followed by a gradual slowing down, ultimately converging in a stable mode. These findings contribute to a better understanding of the effect of frictional resistance on the plunger lift process and provide valuable suggestions for process optimization purposes.
3. Through an analysis and experimental data comparison of five friction coefficient calculation models, it was observed that these models showed significant deviations when describing the annular gap frictional-resistance coefficients in plunger lift systems, making them unable to accurately reflect real-world conditions. This was because the frictional forces within the annular gap were primarily created by the velocity difference between the plunger and liquid column, leading to liquid leakage. These forces are determined by the combined effects of turbulent flow and liquid film friction. Therefore, it is necessary to establish a new model tailored to the annular gap frictional-resistance coefficient to provide a more accurate description of this flow condition.
4. In the vertical wellbore, the model for calculating the annular gap frictional-resistance coefficient showed a negative correlation trend with an increasing Reynolds number, which was more in line with the variation in the annular gap frictional-resistance coefficient during the plunger lift process. Through error calculation methods, such as the coefficient of determination, average absolute percentage error, and root mean square error, the results indicate that the newly proposed model in this paper shows greater accuracy and reliability in predicting the annular gap frictional-resistance coefficient in plunger lift technology.
5. A comprehensive analysis of the simulation results reveals that, when considering the annular gap frictional resistance, the plunger's upward traveling time is close to

the actual traveling time, and the plunger's acceleration shows distinct variations at different stages. Furthermore, through the comparison of the pressure and velocity, it is evident that the annular gap frictional resistance plays a significant role in the plunger's ascent process.

**Author Contributions:** H.S. contributed to the conceptualization, investigation, writing—original draft, programming, analysis, and writing—review and editing. Z.C., R.L. and J.L. (Jie Liu) contributed to the investigation, data curation, and experimentation. J.L. (Junliang Li) contributed to the supervision and validation. S.J. contributed to the experimentation. All authors have read and agreed to the published version of the manuscript.

**Funding:** Funded by National Natural Science Foundation of China, funding number 6223060.

**Data Availability Statement:** Data are contained within the article.

**Conflicts of Interest:** Author Shan Jin was employed by the company of Gui Yang Oil and Gas Transmission Branch of Southwest Pipeline. The remaining authors declare that the research was conducted in the absence of any commercial or financial relationships that could be construed as a potential conflict of interest.

## References

1. Tang, Z.; Li, Y. Liquid Leakage Analysis in Plunger Gas Lifting. *Oil Drill. Prod. Technol.* **2005**, *27*, 44–45.
2. He, S.; Wu, Z. Analyzing the Influence Factors of Plunger Gas Lift and Optimizing Design. *Nat. Gas Ind.* **2005**, *25*, 97–99.
3. Aehengbieke, H. The Plunger Gas Lift Dynamical Model. Ph.D. Thesis, China University of Petroleum, Beijing, China, May 2017.
4. Foss, D.L.; Gaul, R.B. Plunger-Lift Performance Criteria with Operating Experience-Ventura Avenue Field. *Drill. Prod. Pract.* **1965**, *65*, 124–130.
5. Lea, J.F. Dynamic analysis of plunger lift operations. *J. Pet. Technol.* **1982**, *11*, 2617–2629. [[CrossRef](#)]
6. Mower, L.N.; Lea, J.F.; Ferguson, P.L. Defining the Characteristics and Performance of Gas Lift Plungers. In Proceedings of the SPE Annual Technical Conference and Exhibition, Las Vegas, NV, USA, 22 September 1985.
7. Long Felloew, N.; Green, D. Computational fluid dynamics for horizontal well plunger lift system design. In Proceedings of the SPE Western North American and Rocky Mountain Joint Meeting, Denver, CO, USA, 16–18 April 2014.
8. Parsa, E.; Ozkan, E.; Lowery, B.; Cathcart, D.; Lohmann, M. Enhanced plunger lift performance utilizing reservoir modeling. In Proceedings of the SPE Production and Operations Symposium, Oklahoma City, OK, USA, 23–26 March 2013.
9. Hassouna, M. Plunger lift applications: Challenges and economics. In Proceedings of the North Africa Technical Conference and Exhibition, Cairo, Egypt, 15–17 April 2013.
10. Singh, A. Root-cause identification and production diagnostic for gas wells with plunger lift. In Proceedings of the SPE Reservoir Characterization and Simulation Conference and Exhibition, Abu Dhabi, United Arab Emirates, 14–16 September 2015.
11. Moody, L.F. Friction factors for pipe flow. *Am. Soc. Mech. Eng.* **1944**, *66*, 671. [[CrossRef](#)]
12. Wood, D.J. An explicit friction factor relationship. *Civil Eng.* **1966**, *36*, 60–61.
13. Jain, A.K. Accurate explicit equations for friction factor. *J. Hydraul. Div.* **1976**, *102*, 674. [[CrossRef](#)]
14. Churchill, S.W. Friction factor equations spans all fluid-flow regimes. *Chem. Eng.* **1977**, *84*, 91.
15. Chen, N.H. An explicit equation for friction factor in pipe. *Ind. Eng. Chem. Fundam.* **1979**, *18*, 296. [[CrossRef](#)]
16. Li, J.; Yang, H.Z.; Han, M.; Xu, J.C.; Li, X.D.; Han, X.T. Application and Design of Plunger Pump Lifting Viscoelastic Fluid. *Adv. Mater. Res. Vols* **2011**, *291*, 2507–2511.
17. Zhao, K.; Bai, B. Transient liquid leakage during plunger lifting process in gas wells. *J. Nat. Gas Sci. Eng.* **2018**, *59*, 250–261. [[CrossRef](#)]
18. Marsano, L.; Chacin, J. Mechanistic Design of Conventional Plunger Lift Installation. *SPE Adv. Technol. Ser.* **1994**, *2*, 15–24. [[CrossRef](#)]
19. Hernandez, A.; Maracano, L.; Caicedo, S.; Cabunaru, R. Liquid Fall-back Measurements in Intermittent Gas Lift. In Proceedings of the SPE Annual Technical Conference and Exhibition, Houston, TX, USA, 3–6 October 1993.
20. Gupta, A.; Kaisare, N.S.; Nandola, N.N. Dynamic plunger lift model for deliquification of shale gas wells. *Comput. Chem. Eng.* **2017**, *103*, 81–90. [[CrossRef](#)]
21. Wu, Y. The Dynamics Modal Study of Continuous Production Gas Lift Plunger. Ph.D. Thesis, Chengdu University of Technology, Chengdu, China, May 2009.
22. Cao, Y. Simulation and Optimization of Drainage Gas Recovery by Plunger Lift in Highly Deviated Wells. Ph.D. Thesis, Southwest Petroleum University, Chengdu, China, May 2018.
23. Tan, J. Research and Application of Plunger Lifting Technology in Sichuan and Chongqing Area. Ph.D. Thesis, Southwest Petroleum University, Chengdu, China, November 2015.
24. Wang, Q.; Liao, R. The Study of Plunger Motion in Plunger Gas-lift. *J. Basic Sci. Eng.* **2000**, *8*, 89–95.

25. Shi, H.; Liu, J.; Luo, W.; Ding, Y.; Li, R.; Liao, R. Study on Liquid Leakage Model of Rod Plunger Gas Lift. *J. Xi'an Shiyou Univ.* **2022**, *37*, 101–106.
26. Li, Q.; Han, Y.; Liu, X.; Ansari, U.; Cheng, Y.; Yan, C. Hydrate as a by-product in CO<sub>2</sub> leakage during the long-term sub-seabed sequestration and its role in preventing further leakage. *Environ. Sci. Pollut. Res.* **2022**, *29*, 77737–77754. [[CrossRef](#)] [[PubMed](#)]
27. Li, Q.; Wang, F.; Wang, Y.; Forson, K.; Cao, L.; Zhang, C.; Zhou, C.; Zhao, B.; Chen, J. Experimental investigation on the high-pressure sand suspension and adsorption capacity of guar gum fracturing fluid in low-permeability shale reservoirs: Factor analysis and mechanism disclosure. *Environ. Sci. Pollut. Res.* **2022**, *29*, 53050–53062. [[CrossRef](#)] [[PubMed](#)]

**Disclaimer/Publisher's Note:** The statements, opinions and data contained in all publications are solely those of the individual author(s) and contributor(s) and not of MDPI and/or the editor(s). MDPI and/or the editor(s) disclaim responsibility for any injury to people or property resulting from any ideas, methods, instructions or products referred to in the content.